Clays Clay Miner., Vol. 70, No. 1:120–134, 2022
https://doi.org/10.1007/s42860-022-00178-5

ORIGINAL PAPER

Adsorption Behavior of Asphaltene on Clay Minerals and Quartz in a Heavy Oil Sandstone Reservoir with Thermal Damage

Yanlong He · Weizhe Niu · Zhanwu Gao · Hao Dong · Shizi An · Chunchun Han · Liang Zhao

Accepted: 23 February 2022

Abstract Differences in the properties of clay minerals cause formation damage under the condition of thermal production in heavy-oil reservoirs; asphaltenes adsorbed on clay minerals exacerbate the formation damage. The purpose of the present study was to reveal the variation in clay minerals and the adsorption behavior of asphaltenes on clay mineral surfaces under thermal recovery conditions. Volume changes and transformations of typical clay minerals were studied under various conditions (80 and 180°C, pH 9 and 11, aqueous and oven-dry conditions). On this basis, the adsorption behavior and mechanism of asphaltenes on the surfaces of clay minerals in various simulated conditions were investigated. The adsorption mechanism was revealed using kinetics and isothermal adsorption models. The results showed that the volume of montmorillonite expanded by up to 159.13% after water–rock interaction at 180°C with pH 11; meanwhile, the conversion rates of kaolinite and illite to montmorillonite were 6.6 and 7.8%, respectively. The water–rock interaction intensified the volume changes and transformations of clay minerals under thermal conditions. The amounts of asphaltene adsorbed on clay minerals at 180°C were greater than those at 80°C. The adsorption process of asphaltenes was inhibited under aqueous conditions. The abilities of the constituent minerals to bind asphaltenes was in order: montmorillonite > chlorite > kaolinite > illite > quartz sand. The adsorption process of asphaltenes yielded high coefficients of regression with both the Freundlich and Langmuir models under oven-dry (>0.99) and aqueous (>0.98) conditions. At 180°C under aqueous conditions, the water film significantly inhibited the adsorption of asphaltene on the clay minerals. The adsorption process of asphaltenes, therefore, could be regarded as the adsorption occurring at lower concentrations under oven-dry conditions.

Keywords Adsorption kinetics · Asphaltene adsorption · High-temperature steam · Isothermal adsorption model · Water–rock interaction

Y. He · W. Niu · S. An · L. Zhao
School of Petroleum Engineering, Xi'an Shiyou University, Xi'an 710065 Shaanxi, China

Y. He (✉) · W. Niu · S. An · L. Zhao
Key Laboratory of Special Stimulation Technology for Oil and Gas Fields in Shaanxi Province, Xi'an 710065 Shaanxi, China
e-mail: stpnet@126.com

Z. Gao
PetroChina Changqing Oilfield Company, Xi'an 710016 Shaanxi, China

H. Dong
College of Chemistry and Environmental Engineering, Yangtze University, Jingzhou 434023 Hubei, China

C. Han
The 3rd Oil Production Plant, PetroChina Qinghai Oilfield Company, Haixi 816400 Qinghai, China

Introduction

Heavy-oil sandstone reservoirs represent an important oil resource globally and particularly in China (Pang

et al., 2018). The main types of minerals in heavy-oil sandstone reservoirs are quartz, feldspar, and clay minerals, the most common of which are montmorillonite, illite, kaolinite, and chlorite (Hurst & Archer, 1986; Kar et al., 2015; Lopes da Silva et al., 2018). Large montmorillonite and illite contents cause damage easily because of water sensitivity (Baker et al., 1995; Feng et al., 2018; Morodome & Kawamura, 2009; Skipper et al., 1995; Sudhakar & Thyagaraj, 2007). Thermal recovery is currently a major recovery strategy for heavy-oil reservoirs, including cyclic steam stimulation, steam drive, hot water drive, and steam-assisted gravity drainage (Kudrashou & Nasr-El-Din, 2020; Zhao et al., 2014; Zhuang et al., 2018). During steam injection, the water supplied is softened by removing hardness ions such as Ca^{2+} and Mg^{2+}. As the concentrations of Ca^{2+} and Mg^{2+} in the supplied water of the steam generator decrease, the concentration of HCO_3^- increases. During the process of high-temperature and high-quality steam injection, HCO_3^- decomposes into OH^- and CO_2. When CO_2 escapes, the concentration of OH^- in steam condensate increases. The pH of the fluid from the supercritical pressure steam generator is >12. The temperature and pressure of the supercritical pressure steam generator are greater than 374°C and 13.5 MPa, respectively (Afsar & Akin, 2016; Dong et al., 2019). As the steam is injected into the heavy-oil sandstone reservoir, the temperature, pressure, and quality of the steam may decrease. However, the injection of alkaline fluid into the formation by the supercritical pressure steam generator causes complicated water–rock interactions (Bantignies et al., 1997; Herron, 1986). As a result, minerals in the reservoir are dissolved, swell, and fall off easily. Meanwhile, the properties of clay minerals are changed (Sauer et al., 2020). The unfavorable transformation of various clay minerals provides the necessary prerequisite for sensitivity damage. In the processes of thermal recovery, the consequence is reduced permeability and oil recovery of the reservoir (Bentabol et al., 2006; Filipská et al., 2017; Kazempour et al., 2012; Yang et al., 2019; Zhuang et al., 2018).

Asphaltenes are complex, heavy, aromatic molecules present in heavy oil and consist of a polyaromatic core and aliphatic side chains (di Primio et al., 2000; Rogel, 2002). With changes in temperature, pressure, and reservoir fluid properties, asphaltenes are aggregated and deposited easily. The deposited asphaltenes diffuse and adsorb on the surface of clay minerals mainly by coordination bonds, van der Waals forces, and ion exchange (Dean & McAtee Jr., 1986; Rogel, 2002; Wu et al., 2013). However, various factors might affect the adsorption processes, including the structure and characteristics of the clay minerals, the amount and properties of the asphaltenes in the heavy oil, and the existence of a water film preadsorbed on the surface of minerals (Dean & McAtee Jr., 1986; Dubey & Waxman, 1991; Gonzalez & Taylor, 2016; Piro et al., 1996). When the deposited asphaltenes adsorb on the minerals during thermal production, pores are plugged, wettability is reversed, and permeability is decreased, thus exacerbating the thermal damage of the reservoir (Dean & McAtee Jr., 1986; Jafari Behbahani et al., 2013; Kord et al., 2014).

The present study was undertaken to explore the influence of water–rock interactions on the volume changes and transformations of typical clay minerals under oil thermal recovery conditions. On this basis, the adsorption behavior of asphaltenes on the surface of quartz sand and clay minerals under various simulated conditions was analyzed. Another objective was to study the adsorption mechanism under the condition of thermal production by kinetics and isothermal adsorption modeling.

Materials and Methods

Materials

Heavy oil was collected from the Gudong Oilfield Production Plant of Shengli Oilfield, China. The crude oil was characterized by a density of 0.984 g/cm^3. Its viscosity was 4749 mPa s at reservoir temperature (Table 1). The salinities of the formation water, water supplied to the boiler, and steam condensate were 9422.09, 746.03, and 1346.96 mg L^{-1}, respectively (Table 2). Asphaltenes used in this study were extracted by dissolution in toluene and precipitation with *n*-heptane (C7-asphaltenes) according to the method described by Standard SH/T 0266-1992 of China, "Determination of asphaltenes in crude oil" (China Petrochemical Corporation, 1992). $KHCO_3$ was chosen to prepare the simulated steam condensate with a concentration of 1500 mg L^{-1}. NaOH solution was used to regulate the pH values. NaOH and $KHCO_3$, along with toluene, *n*-heptane, and quartz sand (60 and 200 mesh) were purchased from Sinopharm Chemical Reagent Co., Ltd. (Beijing, China). Clay minerals used in this study (200-mesh montmorillonite, illite, kaolinite, and chlorite) were purchased from the resources platform of

https://doi.org/10.1007/s42860-022-00178-5 Published online by Cambridge University Press

Table 1 Properties of crude oil

Property	Density (25°C) (g·cm^{-3})	Viscosity (25°C) (mPa·s)	Saturated hydrocarbons (%)	Aromatic hydrocarbons (%)	Resin (%)	Asphaltene (%)
Value	0.984	4749	34.28	33.64	24.86	6.42

National Standard Materials of China (Beijing Baioubowei Biotechnology Co., Ltd. Beijing, China). Both the quartz sand and clay minerals were all dried at 105°C for more than 24 h before the experiment.

Water–rock Interaction

Four kinds of clay mineral (montmorillonite, kaolinite, chlorite, and illite) were selected to carry out batch experiments under various conditions (80°C, 180°C and pH 9, 11). The standard method for swelling clay minerals was applied according to Standard SY/T 7327-2016 of China, "Shale expansion tester" (National Energy Administration, 2016). The volume changes of the various clay minerals were compared. More specifically, 20 g of each clay mineral (montmorillonite, kaolinite, chlorite, or illite) was weighed and added to a high-temperature, stainless steel reactor (Fig. S1). After leveling and compaction (Table 3), the height of clay (oven-dry) was recorded. Then, 100 mL of simulated steam condensate was added slowly. The suspension was filtered out by a 0.45-μm microporous filter membrane and sand core filter after settling. Meanwhile, the height of the clay (aqueous) was recorded. The reactor was set to 80 or 180°C. After 120 h, the reactor was cooled. The supernatant was filtered by the 0.45-μm microporous filter membrane and sand core filter (Fig. S2). The height of the clay (after the interaction) was measured. The expansion ratio of the clay (E_c) was calculated by applying the following:

$$E_c = \frac{H_r - H_d}{H_d} \times 100 \quad (1)$$

where H_d is the height of oven-dry clay and H_r is the height of the clay cake after the interaction. The remaining samples were dried for 24 h at 110°C. The volume changes of clay minerals under different conditions (80°C, 180°C and pH 9, 11) were analyzed. Furthermore, the transformations of clay minerals before and after the experiment were quantitatively determined using a D/Max 2500v/pc X-ray diffractometer (Rigaku Corporation, Akishima, Tokyo, Japan) (CuKα radiation, 40 kV, 100 mA) following the Chinese Standard SY/T 5163-2010, "Analysis method for clay minerals and ordinary non-clay minerals in sedimentary rocks by the X-ray diffraction" (National Energy Administration, 2016). In order to identify and quantify the clay minerals, X-ray diffraction (XRD) analysis of the mounts was carried out for each sample under natural (air-dried) conditions (N), ethylene-glycol solvation for 24 h in a desiccator (EG), and heating at 550°C for 2 h (H). The compositions of clay minerals were analyzed using the Chinese Standard SY/T5163-1995, "X-ray diffraction analysis method for relative content of clay minerals in sedimentary rocks" (China National Petroleum Corporation, 1995). Finally, the transformations of clay minerals at 180°C with pH 11 were analyzed.

Adsorption of Asphaltenes on Minerals

Quartz sand and clay minerals (montmorillonite, kaolinite, chlorite, and illite) were selected as the adsorbents for the isothermal adsorption experiments. Initially, an asphaltene-toluene solution was used to provide adsorbate under various temperatures (80°C and 180°C) and other conditions (oven-dry and aqueous adsorption).

Table 2 Composition of water

Composition	HCO_3^- (mg·L^{-1})	CO_3^{2-} (mg·L^{-1})	Cl^- (mg·L^{-1})	SO_4^{2-} (mg·L^{-1})	Ca^{2+} (mg·L^{-1})	Mg^{2+} (mg·L^{-1})	K^++Na^+ (mg·L^{-1})	Salinity (mg·L^{-1})	pH
Formation water	635	0	5255.7	29.53	201.17	44.34	3256.35	9422.09	6.9
Water supplied by the boiler	485.24	0	56.62	37.18	0.34	0.58	166.07	746.03	7
Steam condensate	0	376.84	210.21	67.24	0.24	0	692.43	1346.96	12

https://doi.org/10.1007/s42860-022-00178-5 Published online by Cambridge University Press

Toluene was used as an asphaltene-soluble solvent. In toluene, asphaltenes are dispersed at the molecular level. An asphaltene-toluene solution with known concentration (25, 50, 100, 500, and 1000 mg·L^{-1}) was prepared to determine the absorbance value at various wavelengths by UV-Visible spectroscopy; maximum absorption occurred at 295 nm. Based on the Beer-Lambert law, a linear standard calibration curve was obtained for the concentration range of 25 to 1000 mg L^{-1} (Lei et al., 2015; Moreno-Arciniegas & Babadagli, 2014) The adsorption processes at different temperatures (180°C, 80°C) and wet conditions (oven-dry, aqueous) were simulated in the high-temperature, stainless steel reactor. During the oven-dry adsorption process, 20 g of quartz sand, montmorillonite, kaolinite, chlorite, or illite was added to different reactors. Meanwhile, 36 mL of asphaltene-toluene solution with known concentration (0, 25, 50, 75, 100, or 200 mg·L^{-1}) was added. After shaking evenly, the reactor was put into an electric, thermostatic, air-blast drying oven at 180°C or 80°C) for 48 h, after which the absorbance was measured and the concentration of the asphaltene-toluene solution after adsorption was calculated based on the standard curve. Because the Beer-Lambert law applies only in the dilute solution range, solutions with absorbances >0.8 were diluted before measurement. Ultimately, the amount of asphaltenes adsorbed under the various conditions was calculated as the difference between initial and final concentrations:

$$\Gamma = \frac{(C_0 - C) \times V}{m} \tag{2}$$

where Γ is the amount adsorbed (mg g^{-1}), C_0 is the initial concentration (mg L^{-1}), C is the final concentration (mg L^{-1}), V is the volume of the asphaltene-toluene solution, and m is the mass of the mineral. During the aqueous adsorption process, 20 g of quartz sand, montmorillonite, kaolinite, chlorite, or illite was added to the reactor, then 36 mL of deionized water was added to each reactor and allowed to adsorb to the clay for24 h, the excess was removed by a syringe until no flowing water was obvious, and then 36 mL of asphaltene-toluene solution with known concentration (0, 25, 50, 75, 100, or 200 mg L^{-1}) was added to the reactors for adsorption.

Isothermal Adsorption Modeling of Asphaltene on Minerals

The Langmuir isothermal model of adsorption was derived based on thermodynamics and the hypothesis of monolayer coverage of surface sites with uniform adsorption energies (Al-Duri, 1995; Bradley, 1927; Kashefi et al., 2019; Langmuir, 1932; Mansoori Mosleh et al., 2020):

$$\frac{C_e}{Q_e} = \frac{1}{Q_{max} K_L} + \frac{C_e}{Q_{max}} \tag{3}$$

where C_e is the equilibrium concentration of the asphaltene-toluene solution (mg L^{-1}); Q_e is the equilibrium amount of asphaltenes adsorbed by different minerals (mg g^{-1}); Q_{max} is the maximum amount of asphaltenes adsorbed on the surface of minerals (mg g^{-1}); and K_L is the Langmuir constant (L $mmol^{-1}$).

The Freundlich isothermal model of adsorption is an empirical equation applied to surfaces with non-uniform adsorption energies and allows for multilayer adsorption on heterogeneous surfaces (Adams, 2014; Al-Duri, 1995; Daughney, 2000; Dean & McAtee Jr., 1986; Freundlich, 1935; Kashefi et al., 2019).

$$Q_e = K_F C_e^{1/n} \tag{4}$$

where C_e is the equilibrium concentration of the asphaltene-toluene solution (mg L^{-1}); Q_e is the equilibrium adsorption amount of adsorbed by different minerals (mg g^{-1}); K_F is the Freundlich constant; and n is the nonlinear factor.

Results

Volume Changes of Clay Minerals

The volume changes of the clay minerals under simulated steam condensate (Fig. 1, Fig. S4) revealed the expansion ratio of montmorillonite to be more than 110.9%. In particular, at 180°C and pH 11, the expansion ratio reached 159.13%. Montmorillonite showed strong water sensitivity after the water–rock interaction.

Compared with montmorillonite, chlorite was more stable after water–rock interaction. The expansion ratios of chlorite at 180°C with pH 9 and 11 were –3.59 and –7.69%, respectively. However, the expansion ratios of kaolinite at 80°C with pH 9 and pH 11 were 21.30 and

https://doi.org/10.1007/s42860-022-00178-5 Published online by Cambridge University Press

Table 3 Bulk density of the clay minerals

	Oven-dried				Aqueous			
	Montmorillonite	Kaolinite	Chlorite	Illite	Montmorillonite	Kaolinite	Chlorite	Illite
Bulk Density (g/cm^3)	1.12	0.70	0.84	1.47	0.61	1.04	0.93	1.51

47.4%, respectively. For illite, the volume changes were different at 80°C and 180°C. More accurately, at 180°C, the expansion ratio of illite was >48.48%. In particular, for pH 11 at 180°C, the expansion ratio of illite was 58.82%. However, the expansion ratios of illite at 80°C with pH 9 and pH 11 were 13.50% and 16.72%, respectively.

Transformations of Minerals

The XRD spectra of typical clay minerals (montmorillonite, chlorite, kaolinite, and illite) before and after water–rock interaction (Fig. 2 and Table 4) showed the purities of montmorillonite, illite, kaolinite, and chlorite used in the experiment to be 89, 97, 97, and 78%, respectively. Compared with the XRD data (Fig. 2 and Table 4) and the volume changes of clay minerals (Fig. 1, Fig. S4) before and after interaction, the results showed the montmorillonite to be stable at 180°C with pH 11. The amount of montmorillonite decreased from 99.0 to 98.0%. Meanwhile, non-expansive minerals changed (quartz sand decreased from 2.0 to 1.0%, feldspar increased from 8.0 to 10.0%). Kaolinite tended to transform into montmorillonite (6.0%) and illite (1.0%). At the same time, the amount of kaolinite decreased from 97.0 to 90.0%. Correspondingly, the volume changes of kaolinite were reduced by the transformation of montmorillonite at 180°C. At 180°C with pH 11, the expansion ratio of kaolinite was –31.6%. However, the expansion ratio of kaolinite at 80°C reached –47.4%. After the water–rock interaction, illite tended to transform into montmorillonite (the amount of montmorillonite increased by 7.0%). Correspondingly, illite expanded at 180°C (by >48.48%). Chlorite reacted with water to form a small amount of talc (6.0%) and vermiculite (3.0%) under the simulated condition.

Adsorption of Asphaltenes on Minerals

The adsorption kinetics curves of asphaltenes on montmorillonite, chlorite, kaolinite, illite, and quartz sand (Figs. 3 and 4) increased sharply within the first 0.5 h and then tended to stabilize with increasing time. At the same time, the amount of asphaltene adsorbed on 200-mesh quartz sand was greater than that of 60-mesh quartz sand, in both 200- and 400-mg/L asphaltene-toluene solutions. Besides illite, the amount of asphaltene adsorbed on clay minerals was much greater than that on quartz sand. Among them, montmorillonite adsorbed most, followed by chlorite and kaolinite, and the weakest was illite. After 3 h of adsorption, the adsorption processes reached equilibrium. In a 400 mg/L asphaltene-toluene solution, the amounts of asphaltene adsorbed on 200-mesh montmorillonite, illite, kaolinite, chlorite, and quartz sand and 60-mesh

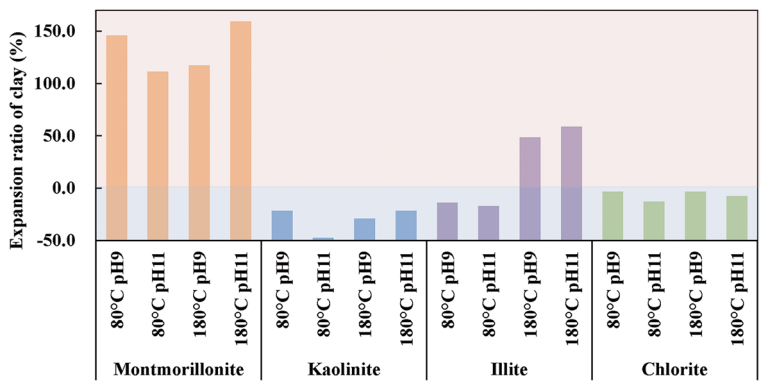

Fig. 1 Volume changes in clay minerals under various conditions

https://doi.org/10.1007/s42860-022-00178-5 Published online by Cambridge University Press

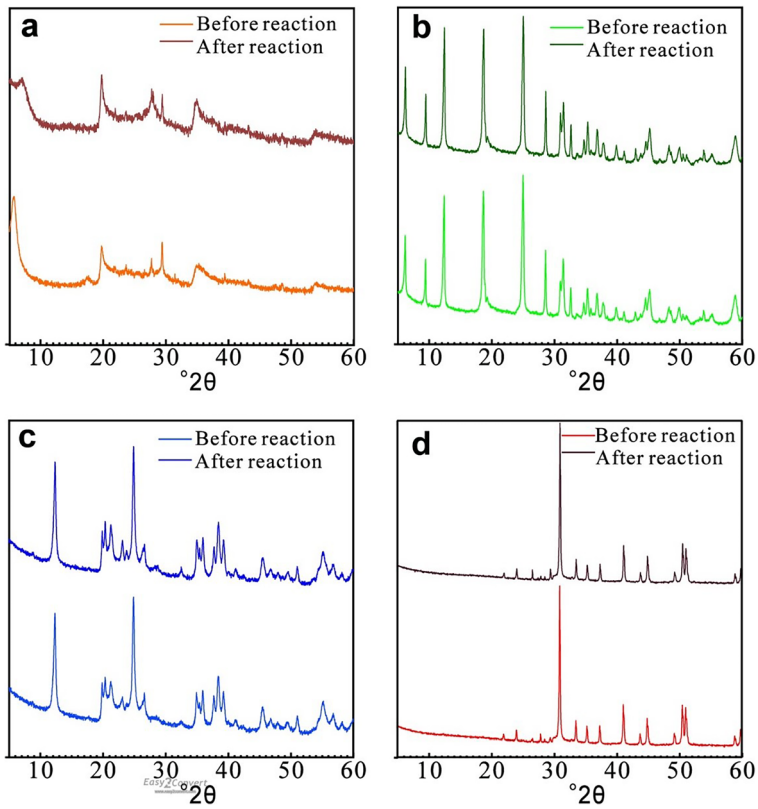

Fig. 2 XRD patterns of clay minerals before and after interaction with asphaltene: **a** montmorillonite; **b** chlorite; **c** kaolinite; **d** illite

quartz sand were 1.22, 0.25, 1.08, 1.15, 0.31, and 0.37 mg g^{-1}, respectively.

The higher the mesh of quartz sand, the smaller the radius and specific surface area, and the greater the adsorption capacity with respect to asphaltenes. The specific surface areas of the clay minerals were larger than that of quartz sand, and the amount of asphaltenes adsorbed on the clay minerals was greater under the same conditions. The amount of asphaltenes adsorbed on the surfaces of quartz sand increased with

Table 4 XRD analysis of clay minerals before and after water–rock interaction

Mineral	Before				After			
	Montmorillonite	Illite	Kaolinite	Chlorite	Montmorillonite	Illite	Kaolinite	Chlorite
Quartz sand (%)	2	–	–	–	1	–	–	–
Feldspar (%)	8	1	–	–	10	2	–	–
Calcite (%)	–	1	–	–	–	–	–	–
Dolomite (%)	–	–	–	8	–	–	–	8
Magnesite (%)	–	–	–	6	–	–	–	6
Talc (%)	–	–	–	7	–	–	–	13
Kaolinite (%)	–	–	97	–	–	–	90	–
Chlorite (%)	–	–	–	78	–	–	–	69
Illite (%)	–	97	1	–	–	90	2	–
Montmorillonite (%)	89	–	–	–	88	7	6	–
Others (%)	1	1	2	1	1	1	2	4

https://doi.org/10.1007/s42860-022-00178-5 Published online by Cambridge University Press

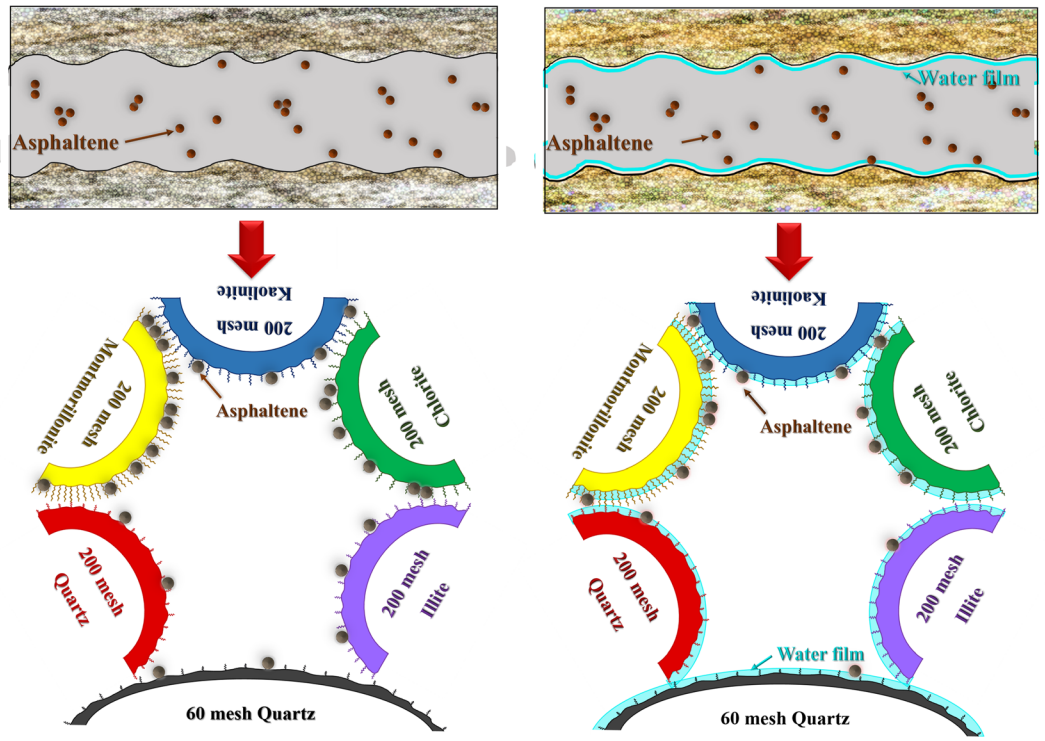

Fig. 3 Asphaltene adsorption processes on mineral surfaces under various conditions and asphaltene concentrations: (left) under oven dry conditions; (right) under aqueous conditions

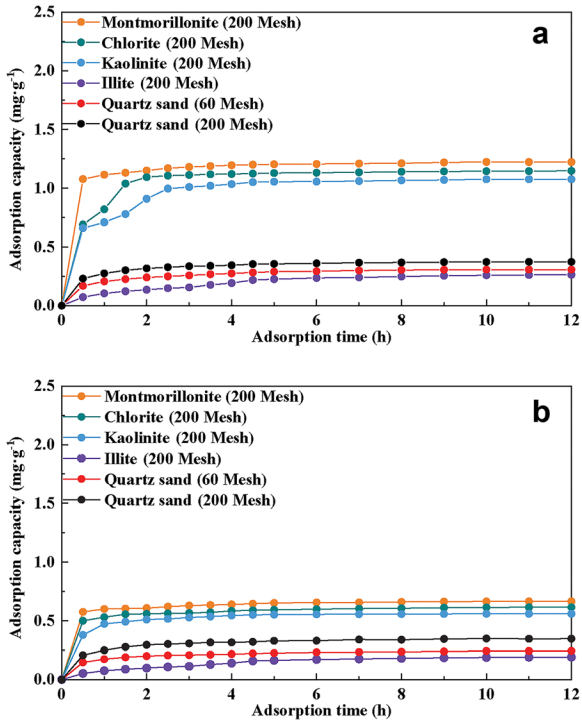

Fig. 4 Adsorption capacity vs. time of asphaltene on the various minerals at **a** 80°C, **b** 180°C

the mesh number under oven-dry conditions at 80°C (Fig. 5). When the adsorption equilibrium concentration of asphaltenes was 867.16 mg L^{-1}, the amount of asphaltene adsorbed on 200-mesh quartz sand was 2.65 mg g^{-1}. At the same time, when the adsorption equilibrium concentration of asphaltenes was 923.67 mg L^{-1}, the amount of asphaltene adsorbed on 60-mesh quartz sand was just 1.66 mg g^{-1}. In addition to illite, the amount of asphaltenes adsorbed on montmorillonite, kaolinite, and chlorite was greater at smaller adsorption equilibrium concentrations. When the adsorption concentration of asphaltenes was 128.77 mg L^{-1}, the amount of asphaltene adsorbed on montmorillonite was 13.54 mg g^{-1}. The amount of asphaltene adsorbed on illite tended to be stable with increased adsorption equilibrium concentration. When the adsorption concentration of asphaltenes was 833.21 mg g^{-1}, the amount of asphaltene adsorbed on illite was just 2.437 mg g^{-1}.

The adsorption equilibrium concentration of asphaltenes had a linear relationship with the adsorption of asphaltenes on the surface of quartz sand under the oven-dry condition at 180°C. Compared with the adsorption process under the oven-dry condition at 80°C,

https://doi.org/10.1007/s42860-022-00178-5 Published online by Cambridge University Press

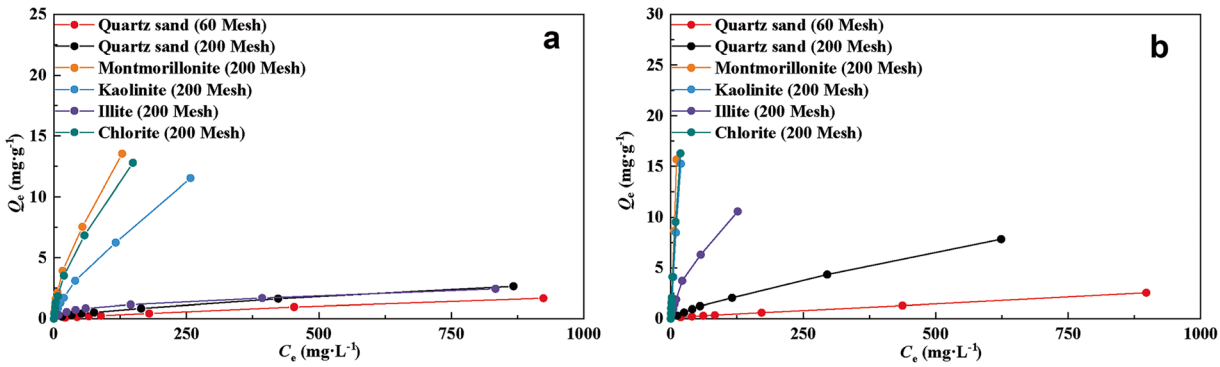

Fig. 5 Adsorption isotherms of asphaltenes on the various minerals under oven-dry conditions at **a** 80°C, **b** 180°C

the adsorption process of asphaltenes on the surface of minerals increased significantly at 180°C. When the concentration of asphaltene solution was 867.16 mg L^{-1}, the asphaltene adsorption amount on 200-mesh quartz sand was 2.65 mg g^{-1} at 80°C. When the concentration of asphaltene solution was 623.58 mg L^{-1}, the asphaltene adsorption amount on 200-mesh quartz sand was 7.83 mg g^{-1} at 180°C. For clay minerals, the amounts of asphaltenes adsorbed on montmorillonite, kaolinite, and chlorite were similar. When the adsorption concentration was 10.827 mg L^{-1}, the asphaltene adsorption amount on montmorillonite reached 15.682 mg g^{-1}. The asphaltene adsorption amount on illite was lower than that of the other three kinds of mineral at 180°C. When the adsorption concentration of asphaltenes was 126.43mg L^{-1}, the amount of asphaltene adsorbed on illite reached 10.57 mg g^{-1}. The isothermal adsorption curves of the four kinds of clay mineral were linear, indicating that these four kinds of clay mineral have strong adsorption capacities under oven-dry adsorption at 180°C.

As the concentration of asphaltenes increased under aqueous conditions at 80°C, the adsorption of asphaltenes on the quartz sand increased. However, the slope of adsorption isotherms decreased gradually, and the adsorption processes tended to be in equilibrium at lower concentrations. The adsorption process of asphaltenes on quartz sand was inhibited by the water film. Water film preadsorbed on minerals showed the strongest inhibition of asphaltene adsorption on the surface of 60-mesh quartz sand (Fig. 6). The rate of inhibition by the water film was least on the 200-mesh quartz sand. When the adsorption concentration of asphaltenes was 896.5 mg L^{-1}, the amount of asphaltene adsorbed on 200-mesh quartz sand was 1.237 mg g^{-1}, and the inhibition rate was >50%. The larger the particle size of quartz sand, the greater the inhibition rate by the water film. At the same time, with increasing asphaltene concentration, the amount of asphaltene adsorbed on the clay minerals also increased, but the adsorption processes stabilized gradually. In particular, the amounts adsorbed on montmorillonite, kaolinite, and chlorite under aqueous conditions were significantly smaller than those under oven-dry conditions. When the adsorption concentration of asphaltenes was 836.4 mg L^{-1}, the amount adsorbed on montmorillonite was only 2.328 mg g^{-1}. When the adsorption concentration of asphaltenes was 896.532 mg L^{-1}, the amount adsorbed on 200-mesh quartz sand was 1.24 mg g^{-1} under aqueous conditions at 80°C. When the adsorption concentration was 941.36 mg L^{-1}, the amount adsorbed on 200-mesh quartz sand was 1.30 mg g^{-1} under aqueous conditions at 180°C. When the adsorption concentration was 836.35 mg L^{-1}, the corresponding amount adsorbed on montmorillonite was 2.18 mg g^{-1} under aqueous conditions at 80°C. When the adsorption concentration of asphaltenes was 567.84 mg L^{-1}, the corresponding amount adsorbed on montmorillonite was 4.98 mg g^{-1} under aqueous conditions at 180°C. At 180°C, the preadsorbed water film could still inhibit asphaltene adsorption on the surface of the clay minerals. However, the inhibition rate was far lower than that at 80°C.

Discussion

Water–rock Interaction

With changing fluid properties, temperature, and pressure, water–rock interaction occurs in various ways. Changes could easily cause the clay minerals to swell and provoke some dissolution, affecting the physical properties of the reservoir and exacerbating reservoir damage. Under

https://doi.org/10.1007/s42860-022-00178-5 Published online by Cambridge University Press

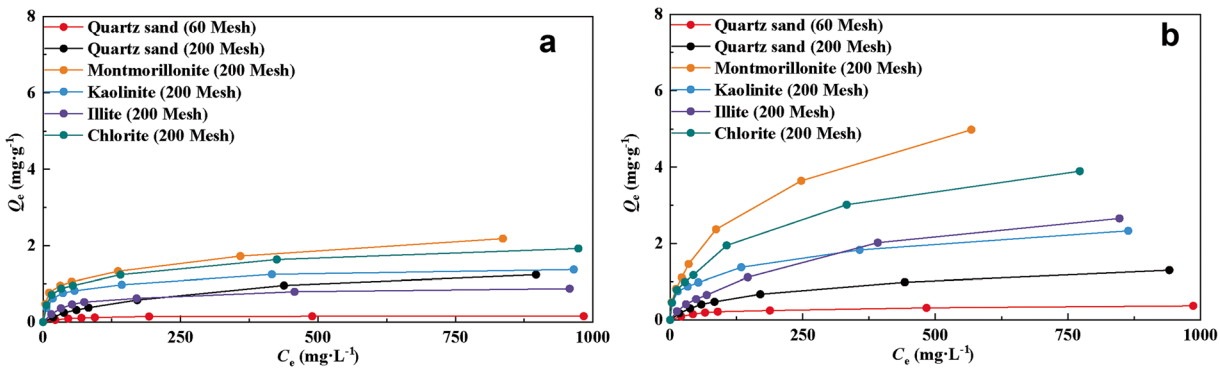

Fig. 6 Adsorption isotherms of asphaltenes on the various minerals under aqueous conditions at **a** 80°C, **b** 180°C

varying reservoir environments, volume changes in clay minerals are caused by their intrinsic properties as well as by their reactions when exposed to water (Kazempour et al., 2012; Kong et al., 2017; Zhuang et al., 2018). In the current study, during thermal production, the salinity of steam condensate was less than that of formation water. After water–rock interaction in steam condensate, the volume expansion of montmorillonite became more obvious. Kaolinite dissolved to varying degrees at higher pH; illite was dissolved mainly at the lower temperature. Both kaolinite and illite, however, tended to transform into montmorillonite under the thermal conditions, and thus also resulted in volume expansion and reservoir damage. Anti-swelling agents, therefore, should be added during steam injection to reduce the adverse effects of water–rock reaction of clay minerals and montmorillonite expansion.

Adsorption Kinetics of Asphaltenes on Clay Minerals

The adsorption of asphaltenes in a reservoir is affected by many factors, such as the environment of the reservoir and the properties of the asphaltenes and the minerals, and by the presence of a water film. The different types of clay minerals have various adsorption sites and capacity. At the beginning of adsorption in the present study, a high concentration of asphaltene-toluene solution was gathered around the adsorption sites on the surface of the clay minerals, which led to increasing surface coverage with time and rates of adsorption thus declined over time as the system approached equilibrium.The adsorption data were fitted to the double-constant rate equation, the parabolic diffusion equation, the Elovich equation, the first-order kinetics equation, and the pseudo-second order kinetics equation (Table 5). The best fit was with the pseudo-second order kinetics equation, the rate-controlling step of which is either chemical reaction or chemisorption. This model encompasses adsorption mechanisms such as external liquid film diffusion, surface adsorption, and intragranular diffusion (Alagumuthu & Rajan, 2010; Bhaumik et al., 2012; El-Khaiary et al., 2010; Hosseini-Dastgerdi & Meshkat, 2019).

Table 5 R^2 values from various kinetics equations for asphaltene adsorption on quartz and the clay minerals (initial concentration of asphaltene = 400 mg·L^{-1})

Mineral	Double-constant rate equation R^2 ($w=at^b$)	Parabolic diffusion equation R^2 ($w=a+bt^{0.5}$)	Elovich equation R^2 ($w=a+b\ln t$)	First-order kinetic equation R^2($\ln w=a+bt$)	Pseudo-second-order kinetic equation R^2 ($t/w=a+bt$)
Quartz sand (60 mesh)	0.9542	0.8787	0.9791	0.6747	0.9640
Quartz sand (200 mesh)	0.9244	0.8177	0.9536	0.6072	0.9849
Montmorillonite (200 mesh)	0.9582	0.8475	0.9644	0.6917	0.8998
Chlorite (200 mesh)	0.6736	0.5196	0.718	0.3459	0.9207
Kaolinite (200 mesh)	0.8196	0.7034	0.8582	0.5082	0.9255
Illite (200 mesh)	0.9578	0.9428	0.9660	0.7679	0.9751

https://doi.org/10.1007/s42860-022-00178-5 Published online by Cambridge University Press

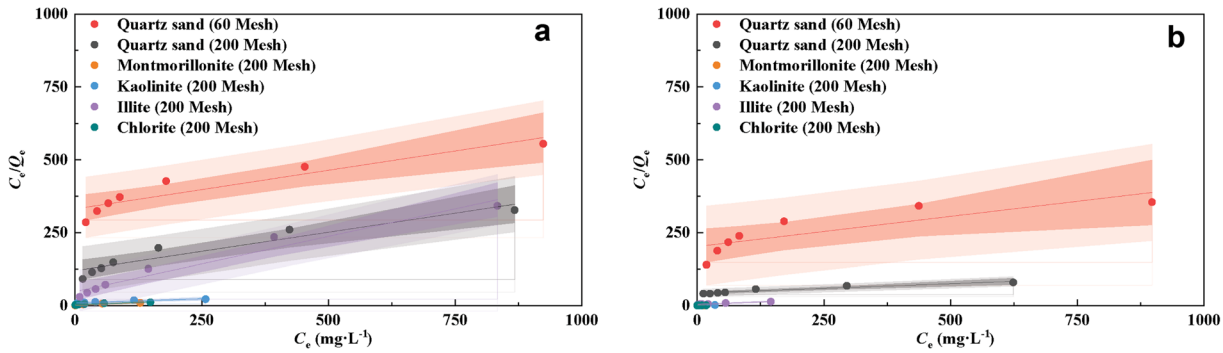

Fig. 7 Langmuir fitting curves of asphaltene adsorbed on the various minerals under oven-dry conditions at **a** 80°C, **b** 180°C

Adsorption Isotherm of Asphaltenes on Clay Minerals

The results from fitting the data to the Langmuir model under different conditions yielded low coefficients of regression (0.7540 to 0.9674) under oven-dry conditions. Under aqueous conditions, however, the regression coefficients were >0.97; in particular the regression coefficient was >0.99 at 80°C (Figs. 7, 8 and Tables 6, 7 and Tables S1 to S12). Under oven-dry condition, the continuous accumulation of macromolecular polar compounds in crude oil formed complex asphaltene aggregates containing surface-active groups with a positive charge and strong polarity (Duran et al., 2019; Rogel, 2002). Surface-active groups on the minerals provided adsorption sites for the strongly polar groups of the asphaltenes by a series of interactions such as dipole-dipole and/or van der Waals forces (Fig. S3) (Dong et al., 2019; Dubey & Waxman, 1991; Wu et al., 2013). Moreover, the water film preadsorbed on the clay mineral surfaces reduced the interaction energy between asphaltenes and clay minerals, thus enabling the water molecules to bind more strongly with the surface. Under these circumstances, water molecules occupied most of the adsorption sites, while the asphaltene molecules were distributed farther from the surfaces (Gonzalez & Taylor, 2016; Li et al., 2017). In particular, the water film homogenized the adsorption sites and made the adsorption of asphaltenes more uniform, which is consistent with the basic hypothesis of the Langmuir model. Furthermore, the rupture of water films was a prerequisite for the adhesion of asphaltenes to a mineral surface. During thermal production, attachment of asphaltene moieties to the surface of clay minerals was irreversible. When protective water films ruptured, water layers which were molecules thick emerged and allowed direct molecular contact of asphaltenes with the mineral surface. With increasing temperature, the forces attracting the water to the clay minerals was overcome and the water molecules were released, which weakened the ability of water films to improve the adsorption capacity of asphaltenes on the clay minerals.

The foregoing results indicate that, under oven-dry conditions, the Langmuir model failed to describe asphaltene adsorption, i.e. the assumptions of single-layer adsorption, uniform adsorbent surface, and uniform adsorption energy do not hold. However, the

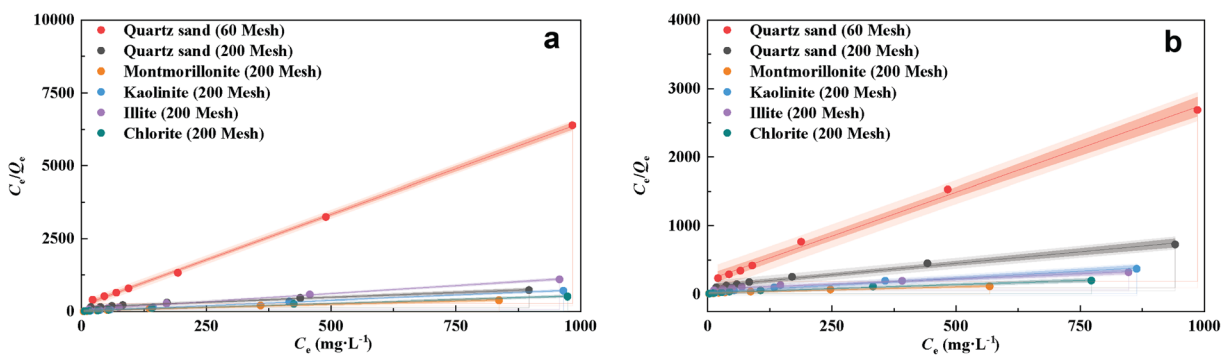

Fig. 8 Langmuir fitting curves of asphaltene adsorbed on the various minerals under aqueous conditions at **a** 80°C, **b** 180°C

https://doi.org/10.1007/s42860-022-00178-5 Published online by Cambridge University Press

Table 6 Langmuir fitting parameters of asphaltenes adsorbed on quartz and clay minerals under oven-dry conditions

Mineral	Temperature (°C)	Condition	Langmuir equation	Q_{max} (mg·g^{-1})	K_L (×10^3)	R^2
Quartz sand (60 mesh)	80	Oven-dry	C_e/Q_e=0.3254C_e+331.37	3.0730	0.9820	0.8736
Quartz sand (200 mesh)	80	Oven-dry	C_e/Q_e =0.2061C_e+120.04	4.8520	1.7170	0.9149
Montmorillonite (200 mesh)	80	Oven-dry	C_e/Q_e =0.0617C_e+2.3108	16.2075	26.7007	0.9357
Kaolinite (200 mesh)	80	Oven-dry	C_e/Q_e =0.0561C_e+9.3475	17.8253	6.0016	0.9290
Illite (200 mesh)	80	Oven-dry	C_e/Q_e =0.3777C_e+48.323	2.6476	7.8162	0.9674
Chlorite (200 mesh)	80	Oven-dry	C_e/Q_e =0.062C_e+3.1734	16.1290	19.5374	0.8489
Quartz sand (60 mesh)	180	Oven-dry	C_e/Q_e =0.207C_e+202.09	4.8309	1.0243	0.7553
Quartz sand (200 mesh)	180	Oven-dry	C_e/Q_e =0.0646C_e+43.044	15.4799	1.5008	0.9172
Montmorillonite (200 mesh)	180	Oven-dry	C_e/Q_e =0.0185C_e+0.8707	54.0541	21.2473	0.7540
Kaolinite (200 mesh)	180	Oven-dry	C_e/Q_e =0.0376C_e+1.0733	26.5957	35.0321	0.7556
Illite (200 mesh)	180	Oven-dry	C_e/Q_e =0.0682C_e+4.2405	14.6628	16.0830	0.8956
Chlorite (200 mesh)	180	Oven-dry	C_e/Q_e =0.0238C_e+0.7147	42.0168	33.3007	0.9486

Langmuir model performed much better under aqueous conditions. The maximum adsorption capacities, according to the Langmuir model, at 80°C under aqueous conditions for the 200-mesh quartz sand, montmorillonite, kaolinite, illite, and chlorite were 1.3890, 2.3364, 1.4486, 1.0129, and 2.0956 mg g^{-1}, respectively. The corresponding maximum amounts of asphaltene adsorbed at 180°C were 1.4848, 5.4825, 2.4195, 3.3636, and 4.1964 mg g^{-1}, respectively.

The results from fitting the data to the Freundlich model (Figs. 9, 10 and Tables 8, 9, Tables S13–S24) revealed that, under oven-dry conditions, the coefficients of regression were greater than 0.99 at both 80 and 180°C. Under aqueous conditions, however, the value was well below 0.99 at 80°C but increased to >0.91 at 180°C. For the clay minerals under oven-dry conditions, 1/*n* was <1, indicating that the adsorption was favorable with good binding and adsorption capacity. For quartz sand, 1/*n* decreased with increasing mesh, indicating that asphaltenes were easier to adsorb with increasing mesh. The greater the K_F value, the stronger the binding ability between adsorbate and adsorbent. Therefore, the larger the mesh of quartz sand, the stronger the binding ability between quartz sand and asphaltenes. Compared with quartz sand, the K_F of the clay minerals was greater than that of quartz sand. Under aqueous conditions, the influence of the water film on the adsorption by the clay minerals weakened with

Table 7 Langmuir fitting parameters of asphaltene adsorbed on quartz and clay minerals under aqueous conditions

Mineral	Temperature/°C	Condition	Langmuir equation	Q_{max}/ mg·g^{-1}	K_L /×10^3	R^2
Quartz sand (60 mesh)	80	Aqueous	C_e/Q_e=6.263C_e+200.02	0.1600	31.3120	0.9996
Quartz sand (200 mesh)	80	Aqueous	C_e/Q_e=0.7197C_e+155.7	1.3890	4.6220	0.9909
Montmorillonite (200 mesh)	80	Aqueous	C_e/Q_e=0.428C_e+22.587	2.3364	18.9490	0.9903
Kaolinite (200 mesh)	80	Aqueous	C_e/Q_e=0.6903C_e+25.96	1.4486	26.5909	0.9988
Illite (200 mesh)	80	Aqueous	C_e/Q_e=0.9873C_e+64.82	1.0129	15.2314	0.9992
Chlorite (200 mesh)	80	Aqueous	C_e/Q_e=0.4772C_e+24.474	2.0956	19.4982	0.9963
Quartz sand (60 mesh)	180	Aqueous	C_e/Q_e=2.5643C_e+207.37	0.3900	12.3658	0.9964
Quartz sand (200 mesh)	180	Aqueous	C_e/Q_e=0.6735C_e+113.82	1.4848	5.9172	0.9903
Montmorillonite (200 mesh)	180	Aqueous	C_e/Q_e=0.1824C_e+14.869	5.4825	12.2671	0.9741
Kaolinite (200 mesh)	180	Aqueous	C_e/Q_e=0.4133C_e+25.76	2.4195	16.0443	0.9858
Illite (200 mesh)	180	Aqueous	C_e/Q_e=0.2973C_e+72.926	3.3636	4.0767	0.9819
Chlorite (200 mesh)	180	Aqueous	C_e/Q_e=0.2383C_e+20.37	4.1964	11.6986	0.9811

https://doi.org/10.1007/s42860-022-00178-5 Published online by Cambridge University Press

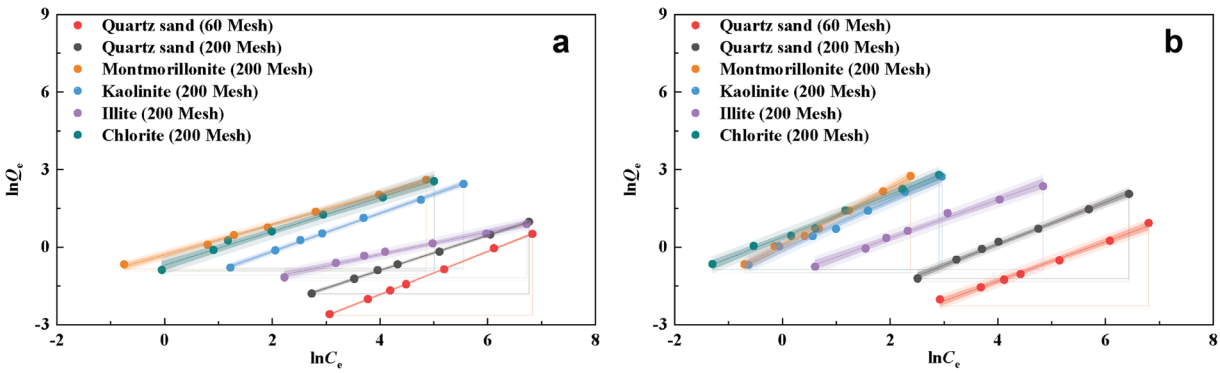

Fig. 9 Freundlich fitting curves of asphaltene adsorbed on the various minerals under oven-dry conditions at **a** 80°C, **b** 180°C

increasing temperature. The water film fell continuously from the surface of the clay minerals under higher temperature. The inhibition of the original water film of the adsorption of asphaltenes was broken, causing more of the non-aqueous adsorption sites to participate in the adsorption process. The adsorption process, therefore, could be regarded as that at lower adsorption concentrations under oven-dry conditions (Fig. 3b).

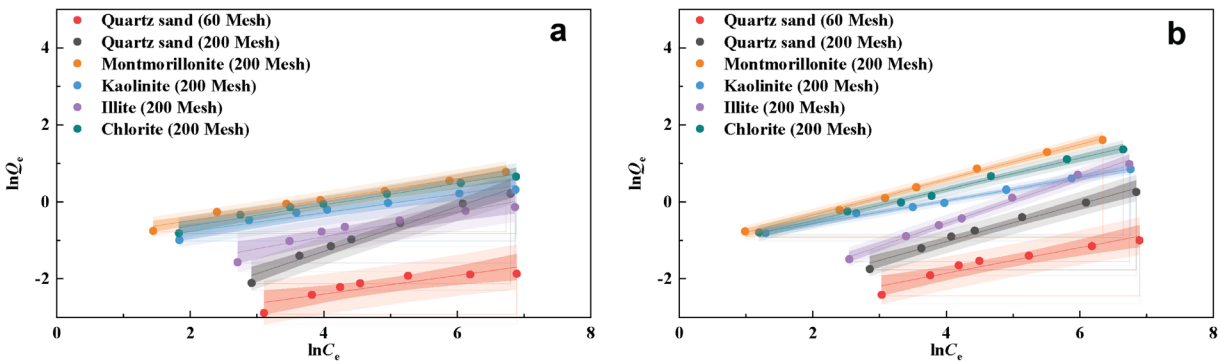

Fig. 10 Freundlich fitting curves of asphaltene adsorbed on the various minerals under aqueous conditions at **a** 80°C, **b** 180°C

Table 8 Freundlich fitting parameters of asphaltene adsorbed on quartz and clay minerals under oven-dry conditions

Mineral	Temperature/°C	Condition	Freundlich equation	n	K_F	R^2
Quartz sand (60 mesh)	80	Oven-dry	$\ln Q_e=0.8266\ln C_e-5.1318$	1.2098	0.0059	0.9998
Quartz sand (200 mesh)	80	Oven-dry	$\ln Q_e=0.679\ln C_e-3.6179$	1.4728	0.0268	0.9995
Montmorillonite (200 mesh)	80	Oven-dry	$\ln Q_e=0.5887\ln C_e-0.3051$	1.6987	0.7370	0.9976
Kaolinite (200 mesh)	80	Oven-dry	$\ln Q_e=0.7402\ln C_e-1.651$	1.3510	0.1919	0.9988
Illite (200 mesh)	80	Oven-dry	$\ln Q_e=0.4378\ln C_e-2.0416$	2.2841	0.1298	0.9908
Chlorite (200 mesh)	80	Oven-dry	$\ln Q_e=0.6578\ln C_e-0.708$	1.5202	0.4926	0.9927
Quartz sand (60 mesh)	180	Oven-dry	$\ln Q_e=0.7609\ln C_e-4.3528$	1.3142	0.0129	0.9942
Quartz sand (200 mesh)	180	Oven-dry	$\ln Q_e=0.8153\ln C_e-3.1541$	1.2265	0.0427	0.9968
Montmorillonite (200 mesh)	180	Oven-dry	$\ln Q_e=0.9455\ln C_e+0.2416$	1.0576	1.2733	0.9954
Kaolinite (200 mesh)	180	Oven-dry	$\ln Q_e=0.7968\ln C_e-0.0374$	1.2550	0.9633	0.9937
Illite (200 mesh)	180	Oven-dry	$\ln Q_e=0.6838\ln C_e-0.9594$	1.4624	0.3831	0.9909
Chlorite (200 mesh)	180	Oven-dry	$\ln Q_e=0.863\ln C_e+0.2127$	1.1587	1.2370	0.9917

https://doi.org/10.1007/s42860-022-00178-5 Published online by Cambridge University Press

Table 9 Freundlich fitting parameters of asphaltene adsorbed on quartz and clay minerals under aqueous conditions

Mineral	Temperature /°C	Condition	Freundlich adsorption isothermal formula	n	K_F	R^2
Quartz sand (60 mesh)	80	Aqueous	$\ln Q_e=0.2432\ln C_e-3.3727$	4.1118	0.0343	0.7912
Quartz sand (200 mesh)	80	Aqueous	$\ln Q_e=0.5808\ln C_e-3.6069$	1.7218	0.0271	0.9792
Montmorillonite (200 mesh)	80	Aqueous	$\ln Q_e=0.2701\ln C_e-1.0255$	3.7023	0.3586	0.9802
Kaolinite (200 mesh)	80	Aqueous	$\ln Q_e=0.2448\ln C_e-1.2627$	4.0850	0.1271	0.9438
Illite (200 mesh)	80	Aqueous	$\ln Q_e=0.3182\ln C_e-2.1763$	3.1427	0.1135	0.9068
Chlorite (200 mesh)	80	Aqueous	$\ln Q_e=0.275\ln C_e-1.1735$	3.6364	0.3093	0.9739
Quartz sand (60 mesh)	180	Aqueous	$\ln Q_e=0.3349\ln C_e-3.1983$	2.9860	0.0408	0.9144
Quartz sand (200 mesh)	180	Aqueous	$\ln Q_e=0.4895\ln C_e-2.9917$	2.0429	0.0502	0.9807
Montmorillonite (200 mesh)	180	Aqueous	$\ln Q_e=0.4571\ln C_e-1.2529$	2.1877	0.2857	0.9964
Kaolinite (200 mesh)	180	Aqueous	$\ln Q_e=0.2985\ln C_e-1.162$	3.3501	0.3129	0.9946
Illite (200 mesh)	180	Aqueous	$\ln Q_e=0.5984\ln C_e-2.9489$	1.6711	0.0524	0.9937
Chlorite (200 mesh)	180	Aqueous	$\ln Q_e=0.4048\ln C_e-1.2965$	2.4704	0.2735	0.9943

The Freundlich model describes adequately the adsorption process of asphaltene under oven-dry and high-temperature aqueous conditions, i.e. non-uniform adsorbent surface, multi-molecular layer adsorption. Under oven-dry conditions, the order of binding abilities between minerals and asphaltenes was as follows: montmorillonite > chlorite > kaolinite > illite > quartz sand (Fig. 3a).

Conclusions

At 180°C and pH 11, the expansion ratio of montmorillonite reached 159.13%. Kaolinite tended to transform into montmorillonite and illite, which reduced the dissolution volume of kaolinite. The conversion rate of illite to montmorillonite was ~7.8% under the high-temperature conditions.

The adsorption process of asphaltene-toluene solution on the surfaces of the various types of minerals was described well by the pseudo-second order kinetics equation. The order of binding abilities between the minerals and the asphaltenes was as follows: montmorillonite > chlorite > kaolinite > illite > quartz sand. The adsorption isotherms for asphaltenes on the four kinds of clay minerals under over-dry conditions at 180°C were linear, indicating strong adsorption capacities and a failure to conform to the assumptions of the Langmuir model.

The adsorption process of asphaltenes on the surfaces of the minerals under aqueous conditions was inhibited because of the formation of a thin water film. At 180°C, the preadsorbed water film still inhibited asphaltene adsorption, but the inhibition rate was far less than at 80°C. Under aqueous conditions, the adsorption process was well fitted by the Langmuir model. Under aqueous conditions at 180°C, the maximum amounts of asphaltene adsorbed on montmorillonite, kaolinite, illite, and chlorite were 1.4848, 5.4825, 2.4195, 3.36, and 4.1964 mg g^{-1}, respectively.

Under the oven-dry and high-temperature aqueous condition, the adsorption process of asphaltenes on the surface of the minerals fitted the Freundlich model well. Under the high-temperature, aqueous conditions, the adsorption process eventually could be regarded as being equivalent to the adsorption of asphaltenes at lower adsorption concentrations under oven-dry conditions.

Acknowledgments This study was supported financially by the National Natural Science Foundation of China (Grant No. 52004216, No. 52004217, No. 51874240, No. 51804256, No. 51804041) and Scientific Research Projects of Shaanxi Provincial Department of Education (No. 20JS119, No. 20JK0829). Shaanxi Province Key Research and Development Plan (No. 2020KW-027).

Funding Funding sources are as stated in the Acknowledgments.

Data Availability All data analysed during this study are included in this published article (and its supplementary information files).Supplementary Information The online version contains

https://doi.org/10.1007/s42860-022-00178-5 Published online by Cambridge University Press

supplementary material available at https://doi.org/10.1007/s42860-022-00178-5.

Declarations

Conflict of Interest The authors declare that they have no conflict of interest.

References

Adams, J. J. (2014). Asphaltene adsorption, a literature review. *Energy & Fuels, 28*(5), 2831–2856. https://doi.org/10.1021/ef500282p

Afsar, C., & Akin, S. (2016). Solar generated steam injection in heavy oil reservoirs: A case study. *Renewable Energy, 91*, 83–89. https://doi.org/10.1016/j.renene.2016.01.047

Al-Duri, B. (1995). A review in equilibrium in single and multicomponent liquid adsorption systems. *Reviews in Chemical Engineering, 11*(2), 101–144. https://doi.org/10.1515/REVCE.1995.11.2.101

Alagumuthu, G., & Rajan, M. (2010). Equilibrium and kinetics of adsorption of fluoride onto zirconium impregnated cashew nut shell carbon. *Chemical Engineering Journal, 158*(3), 451–457. https://doi.org/10.1016/j.cej.2010.01.017

Baker, J. C., Grabowska-Olszewska, B., & Uwins, P. J. R. (1995). ESEM study of osmotic swelling of bentonite from Radzionkow (Poland). *Applied Clay Science, 9*(6), 465–469. https://doi.org/10.1016/0169-1317(95)00002-L

Bantignies, J.-L., Dit Moulin, C. C., & Dexpert, H. (1997). Wettability contrasts in kaolinite and illite clays: Characterization by infrared and X-ray absorption spectroscopies. *Journal de Physique IV France, 7*(C2), 867–869. https://doi.org/10.1051/jp4:1997261

Bentabol, M., Ruiz Cruz, M. D., Huertas, F. J., & Linares, J. (2006). Chemical and structural variability of illitic phases formed from kaolinite in hydrothermal conditions. *Applied Clay Science, 32*(1–2), 111–124. https://doi.org/10.1016/j.clay.2005.12.003

Bhaumik, R., Mondal, N. K., Das, B., Roy, P., Pal, K. C., Das, C., Baneerjee, A., & Datta, J. k. (2012). Eggshell powder as an adsorbent for removal of fluoride from aqueous solution: Equilibrium, kinetic and thermodynamic studies. *Journal of Chemistry, 9*(3), 1457–1480. https://doi.org/10.1155/2012/790401

Bradley, H. (1927). Adsorption isothermals. *Nature, 120*(3011), 82 https://www.nature.com/articles/120082a0.pdf

China National Petroleum Corporation. (1995). *X-ray diffraction analysis method for relative content of clay minerals in sedimentary rocks* (Standard no. SY/T 5163-1995).

China Petrochemical Corporation. (1992). *Determination of asphaltenes in crude oil* (Standard no. SH/T 0266-1992).

Daughney, C. J. (2000). Sorption of crude oil from a non-aqueous phase onto silica: The influence of aqueous ph and wetting sequence. *Organic Geochemistry, 31*(2–3), 147–158. https://doi.org/10.1016/S0146-6380(99)00130-8

Dean, K. R., & McAtee Jr., J. L. (1986). Asphaltene adsorption on clay. *Applied Clay Science, 1*(4), 313–319. https://doi.org/10.1016/0169-1317(86)90008-6

di Primio, R., Horsfield, B., & Guzman-Vega, M. A. (2000). Determining the temperature of petroleum formation from the kinetic properties of petroleum asphaltenes. *Nature, 406*, 173–176.

Dong, X., Liu, H., Chen, Z., Wu, K., Lu, N., & Zhang, Q. (2019). Enhanced oil recovery techniques for heavy oil and oilsands reservoirs after steam injection. *Applied Energy, 239*, 1190–1211. https://doi.org/10.1016/j.apenergy.2019.01.244

Dubey, S. T., & Waxman, M. H. (1991). Asphaltene adsorption and desorption from mineral surfaces. *SPE Reservoir Engineering, 6*(03), 389–395. https://doi.org/10.2118/18462-PA

Duran, J. A., Casas, Y. A., Xiang, L., Zhang, L., Zeng, H., & Yarranton, H. W. (2019). Nature of asphaltene aggregates. *Energy & Fuels, 33*(5), 3694–3710. https://doi.org/10.1021/acs.energyfuels.8b03057

El-Khaiary, M. I., Malash, G. F., & Ho, Y.-S. (2010). On the use of linearized pseudo-second-order kinetic equations for modeling adsorption systems. *Desalination, 257*(1–3), 93–101. https://doi.org/10.1016/j.desal.2010.02.041

Feng, D., Li, X., Wang, X., Li, J., Sun, F., Sun, Z., Zhang, T., Li, P., Chen, Y., & Zhang, X. (2018). Water adsorption and its impact on the pore structure characteristics of shale clay. *Applied Clay Science, 155*, 126–138. https://doi.org/10.1016/j.clay.2018.01.017

Filipská, P., Zeman, J., Všianský, D., Honty, M., & Škoda, R. (2017). Key processes of long-term bentonite-water interaction at 90°C: Mineralogical and chemical transformations. *Applied Clay Science, 150*, 234–243. https://doi.org/10.1016/j.clay.2017.09.036

Freundlich, H. (1935). Adsorptionstechnik. By Franz Krzil. *Journal of Physical Chemistry, 40*(6), 857–858. https://doi.org/10.1021/j150375a022

Gonzalez, V., & Taylor, S. E. (2016). Asphaltene adsorption on quartz sand in the presence of pre-adsorbed water. *Journal of Colloid and Interface Science, 480*, 137–145. https://doi.org/10.1016/j.jcis.2016.07.014

Herron, M. M. (1986). Mineralogy from geochemical well logging. *Clays and Clay Minerals, 34*(2), 204–213. https://doi.org/10.1346/CCMN.1986.0340211

Hosseini-Dastgerdi, Z., & Meshkat, S. S. (2019). An experimental and modeling study of asphaltene adsorption by carbon nanotubes from model oil solution. *Journal of Petroleum Science and Engineering, 174*, 1053–1061. https://doi.org/10.1016/j.petrol.2018.12.024

Hurst, A., & Archer, J. S. (1986). Sandstone reservoir description: An overview of the role of geology and mineralogy. *Clay Minerals, 21*(4), 791–809. https://doi.org/10.1180/claymin.1986.021.4.21

Jafari Behbahani, T., Ghotbi, C., Taghikhani, V., & Shahrabadi, A. (2013). Asphaltene deposition under dynamic conditions in porous media: Theoretical and experimental investigation. *Energy & Fuels, 27*(2), 622–639. https://doi.org/10.1021/ef3017255

Kar, T., Mukhametshina, A., Unal, Y., & Hascakir, B. (2015). The effect of clay type on steam-assisted-gravity-drainage performance. *Journal of Canadian Petroleum Technology, 54*(06), 412–423. https://doi.org/10.2118/173795-PA

Kashefi, S., Lotfollahi, M. N., & Shahrabadi, A. (2019). Asphaltene adsorption using nanoparticles with different surface chemistry: Equilibrium and thermodynamics studies. *Petroleum Chemistry, 59*, 1201–1206. https://doi.org/10.1134/S0965544119110124

Kazempour, M., Sundstrom, E., & Alvarado, V. (2012). Geochemical modeling and experimental evaluation of high-pH floods: Impact of water-rock interactions in sandstone. *Fuel, 92*(1), 2016–2230. https://doi.org/10.1016/j.fuel.2011.07.022

Kong, B., Wang, S., & Chen, S. (2017). Minimize formation damage in water-sensitive Montney formation with energized fracturing fluid. *SPE Reservoir Evaluation & Engineering, 20*(03), 562–571. https://doi.org/10.2118/179019-PA

Kord, S., Mohammadzadeh, O., Miri, R., & Soulgani, B. S. (2014). Further investigation into the mechanisms of asphaltene deposition and permeability impairment in porous media using a modified analytical model. *Fuel, 117*(A), 259–268. https://doi.org/10.1016/j.fuel.2013.09.038

Kudrashou, V. Y., & Nasr-El-Din, H. A. (2020). Formation damage associated with mineral alteration and formation of swelling clays caused by steam injection in sandpacks. *SPE Reservoir Evaluation & Engineering, 23*(01), 326–344. https://doi.org/10.2118/195700-PA

Langmuir, I. (1932). Vapor pressures, evaporation, condensation and adsorption. *Journal of the American Chemical Society, 54*(7), 2798–2832. https://doi.org/10.1021/ja01346a022

Lei, H., Yang, S., Qian, K., Chen, Y., Li, Y., & Ma, Q. (2015). Experimental investigation and application of the asphaltene precipitation envelope. *Energy & Fuels, 29*(11), 6920–6927. https://doi.org/10.1021/acs.energyfuels.5b01237

Li, X., Bai, Y., Sui, H., & He, L. (2017). Understanding the liberation of asphaltenes on the muscovite surface. *Energy & Fuels, 31*(2), 1174–1181. https://doi.org/10.1021/acs.energyfuels.6b02278

Lopes da Silva, M., Martins, J. L., Ramos, M. M., & Bijani, R. (2018). Estimation of clay minerals from an empirical model for cation exchange capacity: An example in Namorado oilfield, Campos Basin, Brazil. *Applied Clay Science, 158*, 195–203. https://doi.org/10.1016/j.clay.2018.02.040

Mansoori Mosleh, F., Mortazavi, Y., Hosseinpour, N., & Khodadadi, A. A. (2020). Asphaltene adsorption onto carbonaceous nanostructures. *Energy & Fuels, 34*(1), 211–224. https://doi.org/10.1021/acs.energyfuels.9b03466

Moreno-Arciniegas, L., & Babadagli, T. (2014). Optimal application conditions of solvent injection into oil sands to minimize the effect of asphaltene deposition: An experimental investigation. *SPE Reservoir Evaluation & Engineering, 17*(04), 530–546. https://doi.org/10.2118/165531-PA

Morodome, S., & Kawamura, K. (2009). Swelling behavior of Na- and Ca-montmorillonite up to 150°C by in situ X-ray diffraction experiments. *Clays and Clay Minerals, 57*, 150–160. https://doi.org/10.1346/CCMN.2009.0570202

National Energy Administration. (2016). *Shale expansion tester* (Standard no. SY/T 7327-2016).

Pang, Z., Lyu, X., Zhang, F., Wu, T., Gao, Z., Geng, Z., & Luo, C. (2018). The macroscopic and microscopic analysis on the performance of steam foams during thermal recovery in heavy oil reservoirs. *Fuel, 233*(1), 166–176. https://doi.org/10.1016/j.fuel.2018.06.048

Piro, G., Canonico, L. B., Galbariggi, G., Bertero, L., & Carniani, C. (1996). Asphaltene adsorption onto formation rock: An approach to asphaltene formation damage prevention. *SPE Production & Facilities, 11*(03), 156–160. https://doi.org/10.2118/30109-PA

Rogel, E. (2002). Asphaltene aggregation: A molecular thermodynamic approach. *Langmuir, 18*(5), 1928–1937. https://doi.org/10.1021/la0109415

Sauer, K., Caporuscio, F., Rock, M., Cheshire, M., & Jové-Colón, C. (2020). Hydrothermal interaction of Wyoming bentonite and opalinus clay. *Clays and Clay Minerals, 68*, 144–160. https://doi.org/10.1007/s42860-020-00068-8

Skipper, N. T., Sposito, G., & Chang, F.-R. C. (1995). Monte Carlo simulation of interlayer molecular structure in swelling clay minerals. 2. Monolayer hydrates. *Clays and Clay Minerals, 43*, 294–303. https://doi.org/10.1346/CCMN.1995.0430304

Sudhakar, M. R., & Thyagaraj, T. (2007). Role of direction of salt migration on the swelling behaviour of compacted clays. *Applied Clay Science, 38*, 113–129. https://doi.org/10.1016/j.clay.2007.02.005

Wu, G., He, L., & Chen, D. (2013). Sorption and distribution of asphaltene, resin, aromatic and saturate fractions of heavy crude oil on quartz surface: Molecular dynamic simulation. *Chemosphere, 92*(11), 1465–1471. https://doi.org/10.1016/j.chemosphere.2013.03.057

Yang, Y., Li, Y., Yao, J., Zhang, K., Iglauer, S., Luquot, L., & Wang, Z. (2019). Formation damage evaluation of a sandstone reservoir via pore-scale X-ray computed tomography analysis. *Journal of Petroleum Science and Engineering, 183*, 106356. https://doi.org/10.1016/j.petrol.2019.106356

Zhao, D. W., Wang, J., & Gates, I. D. (2014). Thermal recovery strategies for thin heavy oil reservoirs. *Fuel, 117*(A), 431–441. https://doi.org/10.1016/j.fuel.2013.09.023

Zhuang, Y., Liu, X., Xiong, H., & Liang, L. (2018). Microscopic mechanism of clay minerals on reservoir damage during steam injection in unconsolidated sandstone. *Energy & Fuels, 32*(4), 4671–4681. https://doi.org/10.1021/acs.energyfuels.7b03686